Performance of ultra-low-dose CT with iterative reconstruction in lung cancer screening – at the same radiation dose as conventional chest X-ray images

Huber Adrian, Landau Julia, Ebner Lukas, Bütikofer Yanik, Leidolt Lars, Brela Barbara, May Michelle, Heverhagen Johannes, Christe Andreas

University Hospital Inselspital Bern, Bern, Switzerland

Corresponding author:

Huber Adrian Thomas

Department of Diagnostic, Interventional and Pediatric Radiology

University Hospital Inselspital Bern

CH-3010 Bern

Phone: +41 31 632 19 65

Fax: +41 31 632 19 15

E-mail: adrian.huber@insel.ch

Abstract

Introduction

This study investigates the detection rate of pulmonary nodules in ultralow-dose CT acquisitions.

Materials and Methods

In this lung phantom study, 232 nodules (115 solid, 117 ground-glass) of different sizes were randomly distributed in a lung phantom in 60 different arrangements. Every arrangement was acquired once with standard radiation dose (100 kVp, 100 references mAs) and once with ultralow radiation dose (80 kVp, 6 mAs). Iterative reconstruction has been used with optimized kernels: I30 for ultralow-dose, I70 for standard dose and I50 for CAD. Six radiologists examined the axial 1 mm stack for solid and ground-glass nodules. During a second and third step, three radiologists used MIP's (maximum intensity projection), finally checking with CAD (computer-assisted detection), while the others first used CAD, finally checking with the MIP's.

Results

The detection rate was 95.5% with standard dose (DLP 126 mGy*cm) and 93.3% with ultralow-dose (DLP: 9 mGy*cm). The additional use of either MIP reconstructions or CAD software could compensate for this difference. A combination of both MIP reconstructions and CAD software resulted in a maximum detection rate of 97.5% with ultralow-dose.

Conclusion

Lung cancer screening with ultralow-dose CT using the same radiation dose as a conventional chest X-ray is feasible.

Key Points

1. 93.3% of all lung nodules were detected with ultralow-dose CT.

2. A sensitivity of 97.5% is possible with additional image post-processing.

3. The radiation dose is comparable to a standard radiography in two planes.

4. Lung cancer screening with ultralow-dose CT is feasible.

Key Words

computed tomography; pulmonary nodule detection; lung adenocarcinoma; ultralow-dose acquisition; diagnostic performance with low radiation dosage.

Abbreviations and acronyms

MIP: Maximum intensity projections

CAD: computer-aided detection

Introduction

Lung cancer accounts for 18% of cancer deaths worldwide. It is the leading cause of cancer deaths in men, and the second leading cause of cancer deaths in women after breast cancer [1]. In 1996, Kaneko et al. showed that conventional chest radiography was inferior to computed tomography for lung cancer screening [2]. Annual CT screening of patients at risk allows for the detection of early-stage lung cancer, which is curable [3]. The National Lung Cancer Screening Trial (NLST) is the first, and so far only, large multicentre study that showed a reduction of 20% in the mortality rate of a high-risk population following annual lung cancer screening, including 53,454 patients [4]. Other large multicentre studies such as the European randomised lung cancer CT screening trial (EUCT) or the Dutch-Belgian randomised lung cancer multi-slice CT screening trial (NELSON) are currently on-going [5, 6]. Now many associations recommend lung cancer screening [7–10].

Nonetheless, since there are some important arguments against lung cancer screening, it is not yet widely applied. The major concerns with lung cancer screening by CT are the costs generated by the repetitive CT acquisitions [11], the high detection rate of false-positive benign nodules [12] and the radiation dose [13]. Smokers and former smokers who receive an annual low-dose CT from the age of 50 to 75 years, with a presumed effective dose of 5.2 mGy per CT acquisition, have a calculated additional risk of 1.8% (95% CI 0.5% - 5.5%) for lung cancer, due to repetitive CT acquisitions [13].

The newest generation of CTs, in combination with iterative reconstruction techniques [14], allow for ultralow-dose CT acquisitions with effective doses similar to the dose of the topogram, and thus, not more than the dose with conventional thoracic radiography in two projections, which is 0.05-0.24 mSv [15]. These ultralow-dose CT acquisitions allow a high sensitivity and diagnostic confidence for the detection of pulmonary nodules [16].

Various secondary read-out tools exist that can increase the detection rate for small lung nodules, such as the use of maximum intensity projections (MIP) [17] or computer-aided detection (CAD) software [18, 19].

The aim of this lung phantom study was to investigate the sensitivity to lung nodules of an ultralow-dose CT with the same effective dose as the dose from conventional radiography, compared to a standard CT alone, as well as in combination with MIP reconstructions and CAD software.

Materials and Methods

Lung phantom preparation and CT acquisition

In this lung phantom study, an anthropomorphic chest phantom (Chest Phantom N1 by Kyoto Kagaku©, 43 x 40 x 48 cm) was used. Thus, approval from the local ethics committee was not necessary. The phantom was equipped with solid (100 HU/5, 8, 10, 12 mm) and ground-glass (-630 HU/5, 8, 10, 12 mm) spherical nodules (size 5, 8, 10 and 12 mm) that were randomly distributed by number, location, type and size to the different lung segments, with a minimum of 0 nodules and a maximum of 8 nodules per phantom. In a total of 60 different phantom arrangements, 232 nodules have been placed, randomly assigned to a lung side, lung segment and peripheral or central location (the inner half of the lung toward the hilum versus the outer half of the lung toward the ribs, radially): 115 were solid, and 117 had a ground-glass density (Figure 1). Five phantoms did not contain any nodules. The phantoms were acquired twice: once with a standard radiation dose, and once with an ultralow radiation dose.

All acquisitions were performed on a Somatom Definition Flash CT (Siemens Forchheim, Germany) featuring iterative reconstruction algorithms (IRIS, Siemens, Germany) and a detector system with integrated readout electronics (Stellar detector, Siemens Forchheim, Germany) with a gantry rotation time of 0.28 seconds. The pitch was 2.2 and the collimation was 0.6 mm. The standard acquisition was performed with 100 kVp in the care-mAs mode with a reference tube-current time product of 100 mAs. The care-kV mode was disabled. For the ultralow-dose acquisition with a tube potential of 80 kVp and a tube current-time product of 6 mAs, care-kV and reference mAs were disabled. These acquisition settings resulted in a volume CT dose index (CTDIvol) of 3.15 mGy for the standard acquisitions and a CTDIvol of 0.22 mGy for the ultralow-dose acquisitions. The corresponding Dose-length product for a scan length of 40 cm was 126 mGy*cm and 9 mGy*cm (Table 1).

The images for both acquisitions were reconstructed in axial stacks with a slice thickness of 1 mm and an increment of 1 mm in a lung parenchyma window (level: -600; window width: 1200), using the vendor specific iterative reconstruction algorithm (iterative reconstruction in imaging space [IRIS]; Siemens, Erlangen, Germany) with the level 3 reconstruction process, integrated in syngo.via, Siemens Healthcare, Erlangen, Germany. Based on data from previous pilot studies, investigating the optimum convolution kernel in ultralow-dose acquisitions [20], radiologists achieved a significantly higher detection rate looking at the 1 mm axial image stack reconstructed with a I30 convolution kernel compared to the I70 convolution kernel normally used in standard CT, while the CAD software performed best with a I50 convolution kernel.

To compare the highest possible detection rates, we consequently used the standard I70 convolution kernel for the standard acquisition, the I30 convolution kernel for the ultralow-dose acquisition and the I50 convolution kernel for the Lung CAD VD10 Mode 2 software. The standard acquisition axial 1 mm stack and the ultralow-dose acquisition axial 1 mm stack were used with the CAD software as well as for the reconstruction with maximum intensity projections (MIP, slice thickness 8 mm, increment 2 mm).

Dose calculation

The effective dose was calculated by multiplying the DLP from the CT protocol with the conversion factors of ICRP 103 [21], which are 0.0147 [mSv/(mGy*cm)] for an adult thoracic CT acquisition with 80 kVp and 0.0144 [mSv/(mGy*cm)] for 100 kVp.

Read-out

The read-out was conducted on a Picture Archiving and Communication System (PACS R11.4.1, 2009; Philips, Best, Netherlands; Sectra, Linkoping, Sweden). A total of six radiologists with 3-7 years of experience in thoracic radiology examined the ultralow-dose and the standard acquisitions in three steps with an interval of at least two weeks between read-out sessions. First, each reader examined the axial 1 mm image stack for solid and ground-glass nodules without any knowledge of additional

MIP's or CAD. The location of the nodules (right/left lung and table position), nodule type (solid/ground-glass) and nodule size (in millimeters) were noted. For the second and third read-out, two groups of readers were formed (three readers each with comparable experience in thoracic imaging between the groups); the first read-out group examined the MIP reconstructions during the second read-out, finally checking with the CAD (third read-out), while the second group used CAD during the second read-out, finally referred to the MIP's (third read-out).

Statistical analysis

The comparisons of nodule detection with standard CT and ultralow-dose CT with and without MIP reconstructions and CAD software were performed with the McNemar test [22]. The differences in the radiation doses between standard and ultralow-dose CT were compared with Wilcoxon's test for paired samples that are not normally distributed [23]. The Chi-square test was applied to the comparison of the central and peripheral locations of the nodules. Sensitivity, specificity, positive predictive value and negative predictive value for lung nodule detection was calculated on a per lung segment basis for the standard-dose and the ultralow-dose acquisitions with and without the additional use of MIP/CAD.

To calculate the inter-reader variability, a non-weighted binary κ-statistic for multiple readers was used by computing the arithmetic mean of the κ-values of each pair of readers (κ-value 0-0.2 poor; 0.21-0.4 fair; 0.41-0.6 moderate; 0.61-0.8 substantial; 0.81-1 almost perfect), using the MedCalc® software [24, 25]. The κ-statistic was performed with and without the additional use of MIP and CAD, once for the standard low-dose CTs and once for the ultralow-dose CTs.

The McNemar test, Wilcoxon's test, the Chi-square test, and the Kappa statistic analysis were performed using MedCalc® software, version 7.6.0.0. (MedCalc Software, Mariakerke, Belgium) [26].

Results

Dose calculation

The estimated effective dose was 1.81 mSv for standard acquisition (DLP: 126 [mGy*cm] * 0.0144 [mSv/(mGy*cm)]) and 0.135 mSv for ultralow-dose acquisition (DLP: 9 [mGy*cm] * 0.0147 [mSv/(mGy*cm)]). The mean effective dose of ultralow-dose acquisition consisted of 0.074 mSv from the acquisition of the topogram alone and only 0.059 from the actual Flash spiral.

Per nodule and per segment analysis

The overall detection rate was 95.5% (± 6.6 % standard deviation) with standard CT and 93.3 % (± 4.3%) with ultralow-dose CT (Table 2). If the read-outs from both standard CT and ultralow-dose CT were enhanced by additional MIP reconstructions, the detection rate was 96.7% (± 3.8%) and 95.4% (± 3.4%), with no significant difference between the two groups. The group that used CAD software detected 99.7% (± 0.4 %) and 97.7% (± 1.4%) of the nodules, with a minimal but significant difference (Table 2). The six readers all together detected a total of 11 false positive nodules on the ultralow-dose acquisitions and a total of 12 false positive nodules on the standard acquisitions, compared to a total of 1357 and 1377 true positive nodules for the standard and ultralow-dose acquisition with the additional use of MIP and CAD. The mean sensitivity, specificity, positive and negative predictive values of all readers are summarized in table 3.

Interreader variability

The κ-statistic showed an almost perfect mean unweighted interreader variability value of κ = 0.91 for the ultralow-dose CT and a mean κ = 0.96 for the ultralow-dose CT with the additional use of MIP and CAD, compared to κ = 0.92 and κ = 0.98 with standard CT.

Influence of nodule size, density and location

While solid nodules had a significantly better detection rate with standard CT (94.2% ± 7.1%) compared to ultralow-dose CT (91.0% ± 6.0%, p-value = 0.006) (Table 4), there was no significant difference between the standard CT (96.9% ± 6.3%) and the ultralow-dose CT (95.6% ± 2.9 %, p-value = 0.188) for the detection of ground-glass nodules (Table 5).

An analysis of the detection rate per nodule diameter showed that only the smallest nodules with diameters of 5 mm were detected at a significantly lower rate with ultralow-dose CT (standard dose 89.9 % ± 18% vs. ultralow-dose 83.9% ± 8.8%; p-value = 0.0075). The lower detection rate of these small nodules using ultralow-dose CT was no longer significant when MIP reconstructions were used (Figure 2), resulting in detection rates of 89.1% ± 6.3% and 93.7% ± 4.5% for ultralow-dose CT when MIP reconstructions and CAD were used, respectively (Table 6). A separate analysis of the ground-glass and the solid nodules per size showed a slight sensitivity drop for the 8 and the 5 mm solid nodules for both standard and ultralow-dose acquisition, while for the ground-glass nodules, a drop of sensitivity was observed just for the smallest 5 mm ground-glass nodules. The 5 mm ground-glass nodules were detected with a similar sensitivity than the 8 mm solid nodules (Table 7).

There was no significant difference in the detection of nodules located in peripheral areas versus central areas (p-value = 0.28).

Combination of MIP and CAD

The combination of MIP and CAD resulted in nodule detection sensitivity of 98.9% (± 2.0%) for standard CT and 97.5% (± 2.5%) for ultralow-dose CT (p = 0.033).

Discussion

The aim of this lung phantom study was to evaluate the lung nodule detection rate in ultralow-dose CT acquisitions using iterative reconstructions, and to investigate the additional use of MIP reconstructions and CAD software.

The overall detection rate of 93.3% for all pulmonary nodules with ultralow-dose acquisition was very similar to the standard acquisition with 95.5%. This small difference could be offset with the use of MIP reconstructions, resulting in a detection rate of 95.4% with ultralow-dose CT, or with the use of CAD software resulting in an even higher detection rate of 97.4% for ultralow-dose CT.

The detection rates in this study were similar to a prior lung phantom study that showed a detection rate of 91% for standard CT acquisition and 97% of standard acquisition with CAD [18], and also to studies investigating CT acquisitions of real patients, such as the study of Veronesi et al. that showed a sensitivity of 90% with a standard lung CT protocol [27]. A recent study by Doo et al, using exactly the same anthropomorphic chest phantom as the present study, investigated the detectability of 5 mm and 8 mm ground-glass nodules (-630 and -800 HU) with a low-dose acquisition and iterative construction (effective does of 0.47 mSv) [28]. The resulting sensitivity of 89 % for 8 mm ground-glass nodules was slightly lower than in the present study (96.2 %). But for the 5 mm ground-glass nodules, there is a striking difference between the results of Doo et al. with a sensitivity of 49 % and the present study, with a sensitivity of 86.7 % (Table 7). One possible explanation for this difference is that in the present study exclusively ground-glass nodules with a density of -630 HU have been used, while Doo et al. also used lower density -800 HU nodules. These smallest 5 mm, very low-density -800 HU ground-glass nodules seem to be very hard to detect with an important drop of sensitivity for the 5 mm ground-glass nodules in the study of Doo et al. However, these very low density ground-glass nodules have not been investigated in the present study.

Detection rates of lung nodules were very high for standard dose as well as for ultralow-dose acquisition, especially when using additional MIP reconstructions or a lung CAD software. While

11

there was not a significantly different detection rate between ultralow-dose CT with MIPs and standard CT with MIPs, ultralow-dose CT with CAD was marginally, but significantly, inferior to standard CT with CAD. In a comparison of MIP's and CAD, MIP's showed a slightly higher added value than CAD in the standard dose setting, while CAD was slightly better in the ultralow-dose setting.

A combination of both MIP reconstructions and CAD software resulted in maximum detection rates of 97.5% for the ultralow-dose acquisitions and of 98.9% for the standard acquisition; thus, there was no real benefit in combining MIP reconstructions and CAD software.

After an analysis of the detection rates of the different sizes of the lung nodules, the only significant difference between the two acquisitions was measured for the smallest nodules (5 mm). These nodules were detected with a sensitivity of 83.9% with ultralow-dose CT, compared to a sensitivity of 89.9% with standard CT. Even in an isolated analysis of the 5 mm nodules, the inferior sensitivity of ultralow-dose CT could be offset by using MIP reconstructions (89.1%) or CAD software (93.7%). Ground-glass nodules in general had a slightly better detection rate than solid nodules, with no significant difference between the standard dose and the ultralow-dose with or without MIP reconstructions / CAD. One possible explanation for this finding was the phantom anatomy itself, in which the lung parenchyma is slightly darker than the usual ground-glass appearance in real patients, depending on how good the patients are able to inspire during CT acquisition. On the other hand, the solid nodules have a very similar density to the underlying artificial broncho-vascular bundles, and are thus probably more difficult to detect. However, studies using CT acquisitions of real patients have also shown a higher detection rate for ground-glass nodules compared to solid nodules, for both human readers and CAD software [29, 30].

This is an interesting point since small solid pulmonary nodules are less likely to be malignant than large solid nodules and ground-glass nodules [31], and thus, small solid nodules show a higher false-positive rate [32]. Additionally, the incidence of lung adenocarcinoma, which often presents as peripheral ground-glass nodules in the early stages, has increased [33].

The slightly inferior detection rate of the small solid 5 mm nodules in ultralow-dose acquisitions could, thus, be acceptable since the relatively low incidence of lung cancer compared to frequently detected lung nodules in a lung cancer screening population, as well as the false positive nodules, are some of the major problems of lung cancer screening.

The Fleischner Society gave recommendations for the management of detected lung nodules depending on nodule size [34], but so far they did not propose how to follow up lung nodules detected in lung cancer screening. There is such a suggestion based on preliminary data of the NELSON CT screening trial, recommending no follow-up for small nodules < 5 mm, follow-up with calculation of volume doubling time for intermediate nodules of 5 − 10 mm, and immediate diagnostic evaluation of large nodules of 10 mm or more [35].

If the ultralow-dose CT is not performed for lung cancer screening but for surveillance of pulmonary metastasis in patients with a known malignancy, detection of very small solid nodules is crucial; thus, ultralow-dose acquisition should be performed at least with additional use of MIP reconstructions or, if available, a lung CAD software.

The NLST showed for the first time a mortality reduction of 20% with lung cancer screening in a high risk screening population (aged 55-74 years with ≥ 30 pack-years of smoking) [4]. Although many associations now recommend lung cancer screening, there are still on-going discussions as well as on-going, large multicentre trials such as the NELSON trial [6]. Nevertheless, Bach et al. calculated that for 2500 screened patients in the NLST with repetitive CT acquisitions, one radiation related cancer death would result [36]. Radiation dose is thus an important issue in a lung cancer screening population because of the cumulative application of radiation dose to the patient's lung with repetitive screening CTs.

With one ultralow-dose CT acquisition of the lung phantom, the effective dose was 0.074 mSv, compared to the 1.81 mSv with standard acquisition. One standard acquisition thus exposed the lung phantom with a higher effective radiation dose than 13 ultralow-dose acquisitions (including

the planning topograms). For the ultralow-dose acquisitions, the topogram even showed a higher effective dose than the actual CT acquisition.

There is an on-going debate on cost-effectiveness with an estimated cost of over U.S. $100,000 per quality-adjusted life-year gained, but could be lowered to U.S. $75,000 if linked to a smoking cessation program [37]. Lung cancer screening results in incidental findings, some of which lead to further investigations, resulting in moderate additional costs of €8.95 [U.S. $12.67] per patient at baseline and €2.25 [U.S. $3.19] at 5-year follow-up [38]. Another point of discussion is the influence of indeterminate baseline screening results on the quality of life of the patients during lung cancer screening [39]. False positive nodules led to biopsy in 1.2% of the patients who were not found to have lung cancer in both the NLST and the NELSON trial [36]. There are new biomarkers to stratify high-risk populations for lung cancer screening, which could result in a better performance of all the discussed points above [40]. But this is a subject of on-going investigations.

A major limitation of this study was the use of a lung phantom, which of course can never fully substitute for the 70 kg Asian man it represents. Moreover, real patients will have individual body constitutions that result in variations in the effective dose. Thus, CT acquisitions of the phantom are comparable to authentic CT acquisitions, but they will never replace CT acquisitions of real patients. Since patients in Europe and America normally weigh 80 kg and more, with many patients weighing over 100 kg, these results may not be applicable to these populations. Thus, the results of this study have to be approved in a real setting.

Another limitation is the different lung convolution kernels used in this study: I70 for standard acquisition, I50 for the lung CAD software and I30 for the ultralow-dose acquisition. This was based on previous pilot studies that proved optimal detection rates with significantly better performance of the lung CAD software with the I50 convolution kernel and a softer I30 convolution kernel for the ultralow-dose acquisition compared to the standard I70 convolution kernel. The softer I30 convolution kernel for the ultralow-dose acquisition helps to compensate the decreased signal-

to-noise ratio of the ultralow-dose acquisitions. Although the use of different convolution kernels might decrease comparability from the strict point of view of systematics, this allows to compare the best possible performance of standard CT, ultralow-dose CT and the CAD software for lung nodules detection, as any radiologist would also try to achieve in a clinical setting with real patients.

Although the two formed read-out groups consisted of radiologists with a comparable experience in thoracic radiology and used the same read-out settings, there are some differences between the two groups. The amount of time that the radiologists spent looking at the images has not been calculated, and there might have been some differences depending on this factor. However, as long as human radiologists are not completely replaced by computer detection software, differences and some small fluctuation will occur. Nevertheless, the interreader variability in this study was very low (almost perfect), and as shown, the additional use of MIP's and CAD helped to lower these effects. This is another argument to use additional MIP-reconstructions or a lung CAD software.

Conclusion

Ultralow-dose CT, using the same dose as a conventional thoracic radiography on two planes, has a comparable sensitivity than standard CT for lung nodule detection, and is thus adequate for lung cancer screening. The small difference in detection rates between ultralow-dose CT and standard CT can be compensated by using MIP reconstructions. The additional use of CAD software results in a slightly higher detection rate for the smallest solid micronodules of 5 mm used in this study. This might be helpful in staging for lung metastases in patients with known cancer, but is not necessarily beneficial in the setting of lung cancer screening, due to a high false positive rate of exactly those small solid micronodules.

Acknowledgments

References

1.   Jemal A, Bray F, Center MM, et al. (2011) Global cancer statistics. CA Cancer J Clin 61:69–90. doi: 10.3322/caac.20107

2.   Kaneko M, Eguchi K, Ohmatsu H, et al. (1996) Peripheral lung cancer: screening and detection with low-dose spiral CT versus radiography. Radiology 201:798–802.

3.   Henschke CI, Yankelevitz DF, Libby DM, et al. (2006) Survival of patients with stage I lung cancer detected on CT screening. N Engl J Med 355:1763–1771.

4.   The National Lung Screening Trial Team (2011) Reduced lung-cancer mortality with low-dose computed tomographic screening. N Engl J Med 365:395–409.

5.   Field JK, van Klaveren R, Pedersen JH, et al. (2013) European randomized lung cancer screening trials: Post NLST. J Surg Oncol 108:280–286. doi: 10.1002/jso.23383

6.   van Iersel CA, de Koning HJ, Draisma G, et al. (2007) Risk-based selection from the general population in a screening trial: selection criteria, recruitment and power for the Dutch-Belgian randomised lung cancer multi-slice CT screening trial (NELSON). Int J Cancer 120:868–874. doi: 10.1002/ijc.22134

7.   Wender R, Fontham ETH, Barrera E, et al. (2013) American Cancer Society lung cancer screening guidelines. CA Cancer J Clin 63:106–117. doi: 10.3322/caac.21172

8.   Jaklitsch MT, Jacobson FL, Austin JHM, et al. (2012) The American Association for Thoracic Surgery guidelines for lung cancer screening using low-dose computed tomography scans for lung cancer survivors and other high-risk groups. J Thorac Cardiovasc Surg 144:33–38. doi: 10.1016/j.jtcvs.2012.05.060

9.   Nair A, Hansell DM (2011) European and North American lung cancer screening experience and implications for pulmonary nodule management. Eur Radiol 21:2445–2454. doi: 10.1007/s00330-011-2219-y

10.   Kauczor H-U, Bonomo L, Gaga M, et al. (2015) ESR/ERS white paper on lung cancer screening. Eur Respir J ERJ–00330–2015. doi: 10.1183/09031936.00033015

11.   Mahadevia PJ, Fleisher LA, Frick KD, et al. (2003) Lung cancer screening with helical computed tomography in older adult smokers: a decision and cost-effectiveness analysis. JAMA J Am Med Assoc 289:313–322.

12. Swensen SJ, Jett JR, Sloan JA, et al. (2002) Screening for lung cancer with low-dose spiral computed tomography. Am J Respir Crit Care Med 165:508–513.

13. Brenner DJ (2004) Radiation risks potentially associated with low-dose CT screening of adult smokers for lung cancer. Radiology 231:440–445. doi: 10.1148/radiol.2312030880

14. Baumueller S, Winklehner A, Karlo C, et al. (2012) Low-dose CT of the lung: potential value of iterative reconstructions. Eur Radiol 22:2597–2606. doi: 10.1007/s00330-012-2524-0

15. Neroladaki A, Botsikas D, Boudabbous S, et al. (2013) Computed tomography of the chest with model-based iterative reconstruction using a radiation exposure similar to chest X-ray examination: preliminary observations. Eur Radiol 23:360–366. doi: 10.1007/s00330-012-2627-7

16. Gordic S, Morsbach F, Schmidt B, et al. (2014) Ultralow-Dose chest computed tomography for pulmonary nodule detection: first performance evaluation of single energy scanning with spectral shaping. Invest Radiol 49:465–473. doi: 10.1097/RLI.0000000000000037

17. Valencia R, Denecke T, Lehmkuhl L, et al. (2006) Value of axial and coronal maximum intensity projection (MIP) images in the detection of pulmonary nodules by multislice spiral CT: comparison with axial 1-mm and 5-mm slices. Eur Radiol 16:325–332. doi: 10.1007/s00330-005-2871-1

18. Christe A, Leidolt L, Huber A, et al. (2013) Lung cancer screening with CT: evaluation of radiologists and different computer assisted detection software (CAD) as first and second readers for lung nodule detection at different dose levels. Eur J Radiol 82:e873–878. doi: 10.1016/j.ejrad.2013.08.026

19. Zhao Y, Bock GH de, Vliegenthart R, et al. (2012) Performance of computer-aided detection of pulmonary nodules in low-dose CT: comparison with double reading by nodule volume. Eur Radiol 22:2076–2084. doi: 10.1007/s00330-012-2437-y

20. Ebner L, Bütikofer Y, Ott D, et al. (2015) Lung Nodule Detection by Microdose CT Versus Chest Radiography (Standard and Dual-Energy Subtracted). Am J Roentgenol. doi: 10.2214/AJR.14.12921

21. ICRP (2007) The 2007 recommendations of the International Commission on Radiological Protection. ICRP publication 103. Ann ICRP 37:1–332. doi: 10.1016/j.icrp.2007.10.003

22. Zar JH (2010) Biostatistical analysis. Prentice-Hall/Pearson, Upper Saddle River, N.J.

23. Wilcoxon F (1946) Individual comparisons of grouped data by ranking methods. J Econ Entomol 39:269.

24. Light RJ (1971) Measures of response agreement for qualitative data: Some generalizations and alternatives. Psychol Bull 76:365–377. doi: 10.1037/h0031643

25. Landis JR, Koch GG (1977) The measurement of observer agreement for categorical data. Biometrics 33:159–174.

26. Schoonjans F, Zalata A, Depuydt CE, Comhaire FH (1995) MedCalc: a new computer program for medical statistics. Comput Methods Programs Biomed 48:257–262.

27. Veronesi G, Maisonneuve P, Spaggiari L, et al. (2014) Diagnostic performance of low-dose computed tomography screening for lung cancer over five years: J Thorac Oncol 9:935–939. doi: 10.1097/JTO.0000000000000200

28. Doo KW, Kang E-Y, Yong HS, et al. (2014) Comparison of chest radiography, chest digital tomosynthesis and low dose MDCT to detect small ground-glass opacity nodules: an anthropomorphic chest phantom study. Eur Radiol 24:3269–3276. doi: 10.1007/s00330-014-3376-6

29. Godoy MCB, Kim TJ, White CS, et al. (2013) Benefit of computer-aided detection analysis for the detection of subsolid and solid lung nodules on thin- and thick-section CT. Am J Roentgenol 200:74–83. doi: 10.2214/AJR.11.7532

30. Li Q, Li F, Doi K (2008) Computerized detection of lung nodules in thin-section CT images by use of selective enhancement filters and an automated rule-based classifier. Acad Radiol 15:165–175. doi: 10.1016/j.acra.2007.09.018

31. Slattery MM, Foley C, Kenny D, et al. (2012) Long-term follow-up of non-calcified pulmonary nodules (<10 mm) identified during low-dose CT screening for lung cancer. Eur Radiol 22:1923–1928. doi: 10.1007/s00330-012-2443-0

32. Henschke CI, Yankelevitz DF, Naidich DP, et al. (2004) CT screening for lung cancer: suspiciousness of nodules according to size on baseline scans. Radiology 231:164–168. doi: 10.1148/radiol.2311030634

33. Travis WD, Brambilla E, Noguchi M, et al. (2011) International Association for the Study of Lung Cancer/American Thoracic Society/European Respiratory Society: International multidisciplinary classification of lung adenocarcinoma. Proc Am Thorac Soc 8:381–385. doi: 10.1513/pats.201107-042ST

34.   MacMahon H, Austin JHM, Gamsu G, et al. (2005) Guidelines for management of small pulmonary nodules detected on CT Scans: a statement from the fleischner society. Radiology 237:395–400. doi: 10.1148/radiol.2372041887

35.   Horeweg N, van Rosmalen J, Heuvelmans MA, et al. (2014) Lung cancer probability in patients with CT-detected pulmonary nodules: a prespecified analysis of data from the NELSON trial of low-dose CT screening. Lancet Oncol 15:1332–1341. doi: 10.1016/S1470-2045(14)70389-4

36.   Bach PB, Mirkin JN, Oliver TK, et al (2012) Benefits and harms of ct screening for lung cancer: a systematic review. JAMA 307:2418–2429. doi: 10.1001/jama.2012.5521

37.   McMahon PM, Kong CY, Bouzan C, et al. (2011) Cost-Effectiveness of CT screening for lung cancer in the U.S. J Thorac Oncol Off Publ Int Assoc Study Lung Cancer 6:1841–1848. doi: 10.1097/JTO.0b013e31822e59b3

38.   Priola AM, Priola SM, Giaj-Levra M, et al. (2013) Clinical implications and added costs of incidental findings in an early detection study of lung cancer by using low-dose spiral computed tomography. Clin Lung Cancer 14:139–148. doi: 10.1016/j.cllc.2012.05.005

39.   Bergh KAM, Essink-Bot M-L, Borsboom GJJM, et al. (2010) Long-term effects of lung cancer CT screening on health-related quality of life (NELSON). Eur Respir J erj01234–2010. doi: 10.1183/09031936.00123410

40.   Vansteenkiste J, Dooms C, Mascaux C, Nackaerts K (2012) Screening and early detection of lung cancer. Ann Oncol 23:x320–x327. doi: 10.1093/annonc/mds303

Figures and Tables

Figure 1: Image comparision (1 mm axial stack): the standard acquisitions (tube voltage: 100 kVp, tube current: 100 mAs, effective dose: 1.81 mSv) with a solid (a) and a ground glass nodule (b) compared to the ultralow-dose acquisitions (tube voltage: 80 kVp, tube current-time product: 6 mAs, effective dose: 0.135 mSv) of the same solid (c) and ground glass nodule (d)

Figure 2: Per nodule diameter analysis: mean sensitivity of standard and ultralow-dose CT with and without assistance of MIP and CAD

Table 1: Acquisition protocol and reconstruction settings for the standard and the ultralow-dose acquisitions

Table 2: The sensitivity of standard and ultralow-dose acquisitions for all lung nodules with and without the assistance of MIP and CAD

Table 3 – The per lung segment analysis of the mean performance of all readers with the sensitivity, the specificity, the positive predictive value and the negative predictive value of standard and ultralow-dose acquisitions including all lung nodules with and without the assistance of MIP and CAD

Table 4: The mean sensitivity of standard and ultralow-dose acquisitions for solid lung nodules with and without the assistance of MIP and CAD

Table 5: The mean sensitivity of standard and ultralow-dose acquisitions for ground glass nodules with and without the assistance of MIP and CAD

Table 6: The per nodule diameter analysis: mean sensitivity of standard and ultralow-dose acquisitions with and without the assistance of MIP and CAD
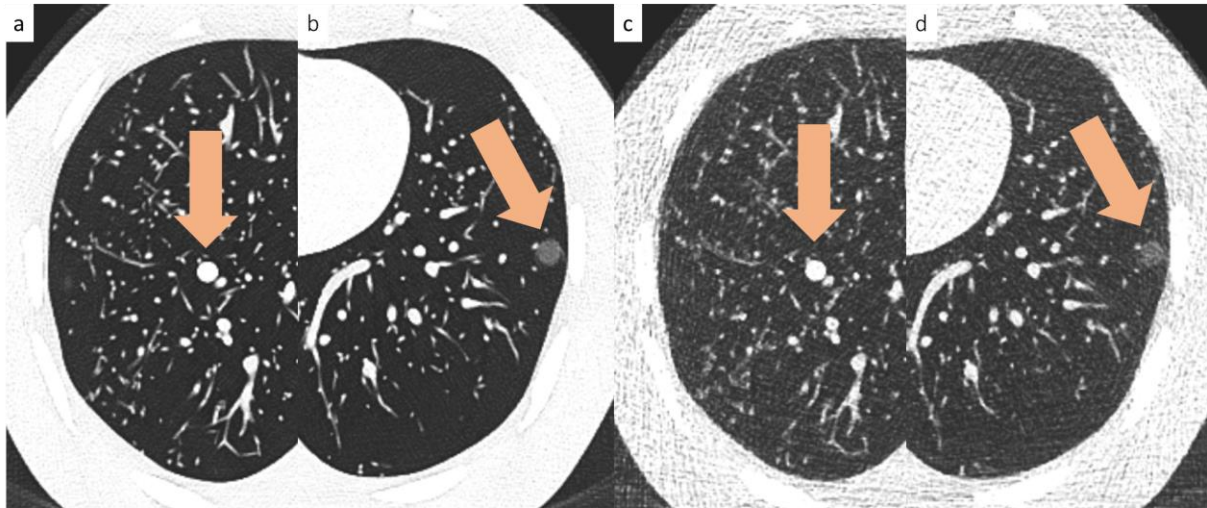
Figure 1 – Image comparision (1 mm axial stack): the standard acquisitions (tube voltage: 100 kVp, tube current: 100 mAs, effective dose: 1.81 mSv) with a solid (a) and a ground glass nodule (b) compared to the ultralow-dose acquisitions (tube voltage: 80 kVp, tube current-time product: 6 mAs, effective dose: 0.135 mSv) of the same solid (c) and ground glass nodule (d).

Table 1 – Acquisition protocol and reconstruction settings for the standard and the ultralow-dose acquisitions

	Standard acquisitions	Ultralow-dose acquisitions
Dose	CTDIvol 3.15 mGy / DLP 126 mGy*cm (40 cm scan-length)	CTDIvol 0.22 mGy / DLP: 9 mGy*cm (40 cm scan length)
Tube voltage	100 kVp	80 kVp
Tube current-time product	100 reference mAs	6 mAs
Primary collimation	0.6 mm	
Gantry rotation time	0.28 seconds	
Pitch	2.2	
Standard readout reconstructions	axial stacks with a slice thickness of 1 mm and an increment of 1 mm in a lung parenchyma window (level: -600; window width: 1200) with an I70 convolution kernel for the standard acquisitions and an I30 convolution kernel for the ultralow-dose acquisitions	
Readout with MIP reconstructions	maximum intensity projection axial stacks with a slice thickness of 8 mm and an increment of 2 mm in a lung parenchyma window (level: -600; window width: 1200) with an I70 convolution kernel for the standard acquisitions and an I30 convolution kernel for the ultralow-dose acquisitions	
Readout with the CAD software	axial stacks with a slice thickness of 1 mm and an increment of 1 mm in a lung parenchyma window (level: -600; window width: 1200) with an I50 convolution kernel	

Table 2 – The sensitivity of standard and ultralow-dose acquisitions for all lung nodules with and without the assistance of MIP and CAD

Groups	Standard acquisitions				Ultralow-dose acquisitions				
	Sensitivity ± SD	Sensitivity with MIP ± SD	p_1	Sensitivity with MIP and CAD ± SD	Sensitivity ± SD	p_2	Sensitivity with MIP ± SD	p_3	p_4	Sensitivity with MIP and CAD ± SD
A	92.2 % ± 8.0 %	96.7 % ± 3.8 %	0.001	98.1 % ± 2.6 %	92.1 % ±4.6 %	1.000	95.4 % ± 3.4 %	0.100	0.025	97.3 % ± 3.3 %
		Sensitivity with CAD					Sensitivity with CAD ± SD			
B	98.9 % ± 0.7 %	99.7 % ± 0.4 %	0.188	99.7 % ± 0.4 %	94.5 % ± 3.5 %	< 0.001	97.7 % ± 1.4 %	0.001	0.007	97.7 % ± 1.4 %
Mean	95.5 % ± 6.6 %			98.9 % ± 2.0 %	93.3 % ± 4.3 %	0.002				97.5 % ± 2.5 %

Both groups started with the 1 mm axial stacks, once looking at the standard acquisitions, once at the ultralow-dose acquisitions. In a second step, for both acquisitions, the readers additionally looked at MIP reconstructions and used a CAD software. While group A first looked at the MIP reconstructions and then checked with the CAD software, group B first used the CAD software, finally checking with the MIP reconstructions.

MIP = maximum intensity projection; CAD = computer-assisted detection; SD = standard deviation; p_1 = standard acquisitions versus standard acquisitions with MIP and CAD; p_2 = axial stack standard acquisitions versus axial stack ultralow-dose acquisitions; p_3 = axial stack ultralow-dose acquisitions versus ultralow-dose acquisitions with MIP and CAD ; p_4 = standard acquisitions with MIP and CAD versus ultralow-dose with MIP and CAD

Table 3 – The per lung segment analysis of the mean performance of all readers with the sensitivity, the specificity, the positive predictive value and the negative predictive value of standard and ultralow-dose acquisitions including all lung nodules with and without the assistance of MIP and CAD

	Standard acquisitions		Ultralow-dose acquisitions	
	Readout without MIP and CAD	Readout with MIP and CAD	Readout without MIP and CAD	Readout with MIP and CAD
Sensitivity ± SD	95.5 % ± 6.6 %	98.9 % ± 2.0 %	93.3 % ± 4.3 %	97.5 % ± 2.5 %
Specificity ± SD	99.8 % ± 0.3 %	99.8 % ± 2.7 %	99.8 % ± 0.3 %	99.8 % ± 0.3 %
PPV ± SD	99.1 % ± 1.1 %	99.1 % ± 0.4 %	99.2 % ± 1.1 %	99.2 % ± 1.0 %
NPV ± SD	98.8 % ± 0.6 %	99.7 % ± 0.3 %	98.2 % ± 0.7 %	99.3 % ± 0.5 %

The readers started with the 1 mm axial stacks, once looking at the standard acquisitions, once at the ultralow-dose acquisitions. In a second step, for both acquisitions, the readers additionally looked at MIP reconstructions and used a CAD software.

MIP = maximum intensity projection; CAD = computer-assisted detection; SD = standard deviation; PPV= positive predictive value; NPV = negative predictive value

Table 4 - The mean sensitivity of standard and ultralow-dose acquisitions for solid lung nodules with and without the assistance of MIP and CAD

Groups	Standard acquisitions			Ultralow-dose acquisitions				
	Sensitivity ± SD	Sensitivity with MIP ± SD	Sensitivity with MIP and CAD ± SD	Sensitivity ± SD	p_1	Sensitivity with MIP ± SD	p_2	Sensitivity with MIP and CAD ± SD
A	90.1 % ± 8.1 %	96.2 % ± 5.3 %	98.0 % ± 2.9 %	88.4 % ± 6.0 %	0.418	93.0 % ± 5.8 %	0.110	96.2 % ± 5.3 %
		Sensitivity with CAD				Sensitivity with CAD ± SD		
B	98.3 % ± 1.5 %	99.4 % ± 0.8 %	99.4 % ± 0.8 %	93.6 % ± 4.7 %	0.001	97.4 % ± 1.4 %	0.581	97.4 % ± 1.4 %
Mean	94.2 % ± 7.1 %		98.7 % ± 2.2 %	91.0 % ± 6.0 %	0.006			96.8 % ± 3.9 %

Both groups started with the 1 mm axial stacks, once looking at the standard acquisitions, once at the ultralow-dose acquisitions. In a second step, for both acquisitions, the readers additionally looked at MIP reconstructions and used a CAD software. While group A first looked at the MIP reconstructions and then checked with the CAD software, group B first used the CAD software, finally checking with the MIP reconstructions.

MIP = maximum intensity projection; CAD = computer-assisted detection; SD = standard deviation; p_1 = standard acquisitions versus ultralow-dose acquisitions; p_2 = standard acquisitions versus ultralow-dose acquisitions with MIP and CAD

Table 5 – The mean sensitivity of standard and ultralow-dose acquisitions for ground glass nodules with and without the assistance of MIP and CAD

Groups	Standard acquisitions			Ultralow-dose acquisitions				
	Sensitivity ± SD	Sensitivity with MIP ± SD	Sensitivity with MIP and CAD ± SD	Sensitivity ± SD	p_1	Sensitivity with MIP ± SD	p_2	Sensitivity with MIP and CAD ± SD
A	94.3 % ± 8.1 %	97.2 % ± 4.0 %	98.3 % ± 2.4 %	95.7 % ± 3.2 %	0.418	97.7 % ± 1.1 %	0.017	98.3 % ± 1.2 %
		Sensitivity with CAD ± SD				Sensitivity with CAD ± SD		
B	99.4 % ± 1.0 %	100.0 % ± 0.0 %	100.0 % ± 0.0 %	95.4 % ± 2.5 %	0.0001	98.0 % ± 1.5 %	0.125	98.0 % ± 1.5 %
Mean	96.9 % ± 6.3 %		99.1 % ± 1.9 %	95.6 % ± 2.9 %	0.188			98.1 % ± 1.3 %

Both groups started with the 1 mm axial stacks, once looking at the standard acquisitions, once at the ultralow-dose acquisitions. In a second step, for both acquisitions, the readers additionally looked at MIP reconstructions and used a CAD software. While group A first looked at the MIP reconstructions and then checked with the CAD software, group B first used the CAD software, finally checking with the MIP reconstructions.

SD = standard deviation; MIP = maximum intensitiy projection; CAD = computer assisted detection; p_1 = standard acquisitions versus ultralow-dose acquisitions; p_2 = standard acquisitions versus ultralow-dose acquisitions with MIP and CAD

Table 6 – The per nodule diameter analysis: mean sensitivity of standard and ultralow-dose acquisitions with and without the assistance of MIP and CAD

5 mm

Nodule size	Standard acquisitions			Ultralow-dose acquisitions				
5 mm	Sensitivity ± SD	Sensitivity with MIP ± SD	Sensitivity with MIP and CAD ± SD	Sensitivity ± SD	p_1	Sensitivity with MIP ± SD	p_2	Sensitivity with MIP and CAD ± SD
A	81.0 % ± 22.1 %	92.0 % ± 10.2 %	96.0 % ± 5.7 %	82.2 % ± 8.6 %	0.864	89.1 % ± 6.3 %	0.020	93.1 % ± 7.3 %
		Sensitivity with CAD ± SD	Sensitivity with MIP and CAD ± SD			Sensitivity with CAD		Sensitivity with MIP and CAD
B	98.9 % ± 1.0 %	100 % ± 0.0 %	100.0 % ± 0.0 %	85.6 % ± 8.6 %	<0.001	93.7 % ± 4.5 %	0.12	93.7 % ± 4.5 %
Mean	89.9 % ± 18 %		98.0 % ± 4.5 %	83.9 % ± 8.8 %	0.008			93.4 % ± 6.1 %

8 mm

Nodule size	Sensitivity ± SD	Sensitivity with MIP ± SD	Sensitivity with MIP and CAD ± SD	Sensitivity ± SD	p_1	Sensitivity with MIP ± SD	p_2	Sensitivity with MIP and CAD
A	92.4 % ± 6.0 %	97.1 % ± 3.0 %	98.2 % ± 2.5 %	90.1 % ± 6.5 %	0.424	95.3 % ± 4.4 %	0.227	98.2 % ± 2.5 %
		Sensitivity with CAD ± SD	Sensitivity with MIP and CAD ± SD			Sensitivity with CAD ± SD		Sensitivity with MIP and CAD
B	97.7 % ± 1.0 %	99.4 % ± 0.8 %	99.4 % ± 0.8 %	94.2 % ± 3.3 %	0.070	98.2 % ± 0.0 %	1.000	98.2 % ± 0.0 %
Mean	95.0 % ± 5.0 %		98.8 % ± 1.9 %	92.1 % ± 5.5 %	0.052			98.2 % ± 1.8 %

10 mm

Nodule size	Sensitivity ± SD	Sensitivity with MIP ± SD	Sensitivity with MIP and CAD ± SD	Sensitivity ± SD	p_1	Sensitivity with MIP ± SD	p_2	Sensitivity with MIP and CAD ± SD
A	96.3 % ± 5.2 %	97.5 % ± 3.5 %	97.5 % ± 3.5 %	98.8 % ± 1.7 %	0.219	98.8 % ± 1.7 %	0.219	98.8 % ± 1.7 %
		Sensitivity with CAD ± SD	Sensitivity with MIP and CAD ± SD			Sensitivity with CAD		Sensitivity with MIP and CAD ± SD
B	99.4 % ± 1.1 %	100 % ± 0.0 %	100.0 % ± 0.0 %	99.4 % ± 0.9 %	1.000	99.4 % ± 0.9 %	1.00	99.4 % ± 0.9 %
Mean	97.8 % ± 4.1 %		98.8 % ± 2.8 %	99.1 % ± 1.4 %	0.289			99.1 % ± 1.4 %

12 mm

Nodule size	Sensitivity ± SD	Sensitivity with MIP ± SD	Sensitivity with MIP and CAD ± SD	Sensitivity ± SD	p1	Sensitivity with MIP ± SD	p2	Sensitivity with MIP and CAD ± SD
A	98.4 % ± 0.0 %	99.5 % ± 0.7 %	100.0 % ± 0.0 %	97.4 % ± 2.0 %	0.688	98.4 % ± 1.3 %	1.000	98.9 % ± 1.5 %
		Sensitivity with CAD ± SD	Sensitivity with MIP and CAD ± SD			Sensitivity with CAD		Sensitivity with MIP and CAD ± SD
B	99.5 % ± 0.9 %	99.5 % ± 0.7 %	99.5 % ± 0.7 %	98.9 % ± 1.5 %	1.000	99.5 % ± 0.7 %	1.000	99.5 % ± 0.7 %
Mean	99.2 % ± 0.8 %		99.7 % ± 0.6 %	98.1 % ± 1.9 %	0.508			99.2 % ± 1.2 %

Both groups started with the 1 mm axial stacks, once looking at the standard acquisitions, once at the ultralow-dose acquisitions. In a second step, for both acquisitions, the readers additionally looked at MIP reconstructions and used a CAD software. While group A first looked at the MIP reconstructions and then checked with the CAD software, group B first used the CAD software, finally checking with the MIP reconstructions.

SD = standard deviation; MIP = maximum intensity projection; CAD = computer-assisted detection; A = group a, readout order 1. CT 2. MIP; B = group b, readout order 1. CT 2. CAD; p_1 = standard acquisitions versus ultralow dos acquisitions; p_2 = standard dose acquisitions versus ultralow dos acquisitions with MIP and CAD

Table 7 – The per nodule diameter analysis: mean sensitivity of ground-glass and solid nodules without additional MIP / CAD

Nodule size	Ground-glass nodules		Solid nodules	
	Ultralow dose acquisition	Standard acquisition	Ultralow dose acquisition	Standard acquisition
5 mm	86.7 % ± 9.0 %	90.6 % ± 21.1 %	81.0 % ± 9.1 %	89.3 % ± 15.2 %
8 mm	96.7 % ± 3.8 %	97.8 % ± 3.0 %	87.0 % ± 10.6 %	92.0 % ± 8.7 %
10 mm	100.0 % ± 0.0 %	98.6 % ± 3.1 %	98.3 % ± 2.5 %	97.2 % ± 4.9 %
12 mm	100.0 % ± 0.0 %	100.0 % ± 0.0 %	96.4 % ± 3.8 %	97.9 % ± 1.5 %

The mean sensitivity per ground-glass and solid nodule size of both groups looking at the 1 mm axial stacks, once acquired with standard dose, once with ultralow-dose.
SD = standard deviation